



# Microstructure evolution of TC4 titanium alloy/316L stainless steel dissimilar joint vacuum-brazed with Ti-Zr-Cu amorphous filler metal

Yueqing Xia<sup>1</sup> · Honggang Dong<sup>1</sup> · Xiaohu Hao<sup>1</sup> · Shuai Li<sup>1</sup> · Peng Li<sup>1</sup> · Guoshun Yang<sup>2</sup>

Received: 15 January 2018 / Accepted: 18 January 2019 / Published online: 29 January 2019  
© International Institute of Welding 2019

## Abstract

TC4 titanium alloy was vacuum-brazed to 316L stainless steel (SS) with Ti-Zr-Cu amorphous filler metal. The effect of brazing time and temperature on the interfacial microstructure and mechanical properties of joints was investigated. Electron probe micro-analyzer (EPMA) and scanning electron microscopy (SEM) equipped with energy dispersive spectroscopy (EDS) were used to study the joint microstructure; meanwhile, the reaction phases on fracture surfaces were identified by X-ray diffraction (XRD). The results show that all joints had similar interfacial microstructure of TC4 titanium substrate/Widmanstätten/ $\beta$ -Ti + Ti<sub>2</sub>Cu/( $\alpha$ -Ti +  $\lambda$ -Cu<sub>2</sub>TiZr) + Ti<sub>2</sub>Cu/Ti-Fe-Cu/TiFe/(Fe, Cr)<sub>2</sub>Ti/ $\sigma$ -phase + Fe<sub>ss</sub>/316L stainless steel substrate. Three reaction layers TiFe/(Fe, Cr)<sub>2</sub>Ti/ $\sigma$ -phase + Fe<sub>ss</sub> formed close to 316L stainless steel substrate and could benefit the mechanical properties of joints. The maximum shear strength of 65 MPa was obtained at 950 °C for 10 min. During shear test, cracks initiated at the interface of Ti-Cu-Fe layer/TiFe layer and propagated along the brazed seam/316L interface with a large amount of cleavage facets existing on the fracture surface.

**Keywords** Vacuum brazing · Ti-Zr-Cu amorphous filler metal · Interfacial microstructure · Intermetallic compound (IMC) · Shear strength

## 1 Introduction

With excellent specific strength and exceptional corrosion resistance, titanium alloys are widely used in aerospace and chemical engineering industries [1, 2]. For the purpose of weight reduction, cost saving, and mechanical structural functions, joining titanium (alloy)/stainless steel is becoming more and more attractive. Joining of titanium (alloy)/stainless steel is mainly performed with friction welding [3–5], diffusion welding [6–9], explosive welding [10–12], laser welding [13, 14], and electron beam welding [15, 16] processes. However, compared with brazing process, the above welding processes have disadvantages, such as high cost and process

inflexibility. Ag-based and Ti(Zr)-based filler metals are mostly used in brazing titanium (alloy)/stainless steel. The joints brazed with Ti-based filler metals have excellent corrosion resistance and elevated temperature resistance [17]. With the significant development of rapid cooling technology, most of Ti-based filler metals can be fabricated into amorphous foils which are more flexible for brazing. Compared with crystalline filler metals, amorphous filler metals are more homogeneous and have much narrower melting range. While brazing Ti (Gr. 2)/UNSS 31254 using 41.2Zr-13.8Ti-10.0Ni-12.5Cu-22.5Be (at%) amorphous filler metal [18], cracks initiated in brittle IMCs (Ti-Ni, Ti-Fe) and propagated along the boundary between the IMCs and matrix. Continuous brittle NiTi<sub>2</sub> and  $\sigma$ -phase were observed at the interface of brazed seam/UNSS 31254 at 900 °C. Cui et al. [19] used Zr-Ti-Ni-Cu amorphous filler metal with different constituents to braze TA2 titanium alloy/Q235 steel. TiC, TiFe, and TiFe<sub>2</sub> phases were found on the fracture surfaces with the highest shear strength of 139 MPa. In our previous research, Ti-22Ni-10Cu-8Zr [20] and Cu-Ti-Ni-Zr-V [21] filler metals were used to braze titanium alloy/steel. With addition of V, the shear strength of joints significantly increased from 30 MPa to more than 100 MPa. However, a large amount of Ti-based IMCs (Ti-Al, Ti-Fe-Cu, and Ti-Ni) formed in the brazed seam.

Recommended for publication by Commission XVII - Brazing, Soldering and Diffusion Bonding

✉ Honggang Dong  
donghg@dlut.edu.cn

<sup>1</sup> School of Materials Science and Engineering, Dalian University of Technology, Dalian 116024, People's Republic of China

<sup>2</sup> Shanghai Aerospace Equipment Manufacturer, Shanghai 200245, People's Republic of China

According to Ref. [6], V has good compatibility with most elements of the base metals and filler metals. Thus, the formation of intermetallic compounds would be reduced, which is beneficial for promoting the mechanical properties of joints. However, the research on the brazing of titanium alloy/stainless steel with Ti (Zr)-based filler metal is still insufficient.

In this paper, Ti-25Zr-50Cu (wt%) amorphous filler metal was fabricated to braze TC4 titanium alloy to 316L stainless steel. The effect of brazing time and temperature on shear strength and evolution of microstructure was investigated. The typical reaction phases were characterized and the fracture mechanism of TC4/Ti-25Zr-50Cu/316L joints was analyzed.

## 2 Experimental procedure

### 2.1 Materials

TC4 (Ti-6Al-4V) titanium alloy and SUS 316L stainless steel sheets with thickness of 2 mm were used as base metals. Their chemical composition is listed in Table 1, and the microstructure of the matrix is displayed in Fig. 1. It can be seen that 316L stainless steel consists of blocky  $\gamma$ -Fe phase, while TC4 titanium alloy is composed of blocky  $\alpha$ -Ti phase surrounded with  $\beta$ -Ti phase. The brazed specimens were machined into dimensions of 60 mm  $\times$  15 mm  $\times$  2 mm with electrical discharge machining.

Prior to fabricating filler metal, Ti-25Zr-50Cu (wt%) alloy ingot was prepared by arc remelting and the filler metal was fabricated by melt spinning under  $5 \times 10^{-3}$  Pa vacuum atmosphere. The produced filler foil is 4–5 mm in width and 90–100  $\mu$ m in thickness.

### 2.2 Brazing

Before brazing, the specimens were ground with 600# grit SiC paper, then ultrasonically cleaned in acetone bath for 15 min, rinsed with deionized water, and finally dried by air blowing. As the assembly of brazed samples shown in Fig. 2, the overlap width was 5 mm. A pressure of 20 kPa was employed with a graphite block to ensure the tight contact of the faying surfaces. The brazing of TC4 titanium alloy/Ti-25Zr-50Cu/316L stainless steel was carried out in a vacuum brazing furnace with the vacuum of  $\sim 5 \times 10^{-3}$  Pa. The time-temperature

heating curve is shown in Fig. 3. In the first stage of brazing process, the specimens were heated to 800 °C at a faster heating rate of 10 °C/min and then held for 5 min. Subsequently, the specimens were heated to the brazing temperature at a smaller rate of 5 °C/min to keep the temperature of the brazed samples uniform. The brazed samples were held for the brazing duration time after reaching the target temperature. Finally, the couples were cooled down to room temperature in the furnace. The brazing temperature varied from 890 to 950 °C with an interval of 20 °C. Brazing process depends on the reactive wetting between filler metal and base metal. Once the filler metal begins to melt, chemical reaction within the joint would occur. To prevent the excessive growth of intermetallic compounds, which might deteriorate the joint properties, the holding time for each brazing temperature was 5, 10, and 15 min. After vacuum brazing, the metallographic samples were gradually ground with up to 2000# SiC paper and then polished with 1.5  $\mu$ m diamond polishing paste. To examine the microstructure of base metals, TC4 titanium alloy was etched with Kroll reagent (2 mL HF + 4 mL HNO<sub>3</sub> + 94 mL H<sub>2</sub>O, vol%) and 316L stainless steel was etched by electrolytic etching with dipping in the electrolyte (10 g oxalic acid + 100 mL H<sub>2</sub>O) for 20 s under the voltage of 6 V.

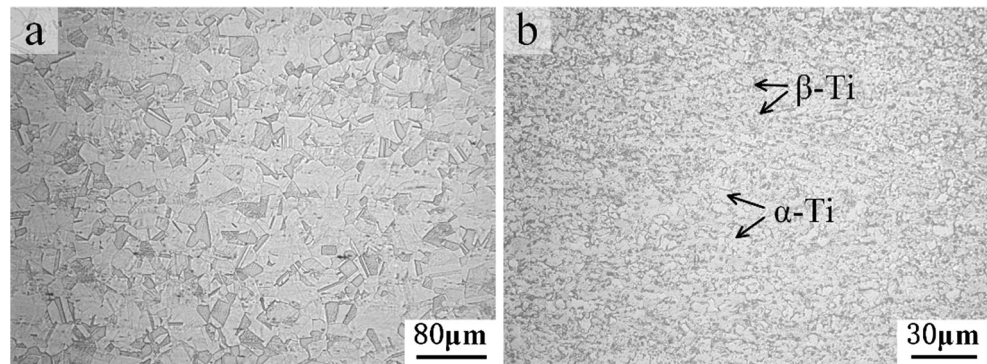
### 2.3 Characterization

X-ray diffraction (XRD, Empyrean) with Co-K $\alpha$  radiation and electron probe micro-analyzer (EPMA-1600, Shimadzu, Japan) were used to characterize the microstructure of the filler foil. The thermal behavior of filler metal was examined using a differential thermal analysis device (DTA, TA Q600) with a heating rate of 20 °C/min. After vacuum brazing, the shear test of brazed joints was conducted by a DNS-100 universal tensile testing machine at a crosshead speed of 0.5 mm/min. Three identical shear samples were employed to obtain the average shear strength for each brazing parameter. The microstructure of base metals was examined by LEICA MEF4A optical microscope (OM). ZEISS-SUPRA55 field emission scanning electron microscope (SEM) equipped with energy dispersive spectroscopy (EDS) was used to investigate the microstructure and fracture surfaces of brazed joints. Phase observation and composition analysis (elemental quantitative analysis, line scanning, and map scanning) of the brazed seams were performed by EPMA and SEM. Moreover, XRD was used to examine phase constituents and structure on the fracture surfaces.

**Table 1** Chemical composition of base metals (wt%)

Base metals	Cr	Ni	Mo	Mn	Al	V	Other elements	Ti	Fe
316L	16.5	10.2	2.0	1.3	–	–	<1.0	–	Bal.
TC4	–	–	–	–	5.9	3.6	<0.2	Bal.	–

**Fig. 1** Microstructure of base metals **a** 316L stainless steel; **b** TC4 titanium alloy



### 3 Results and discussion

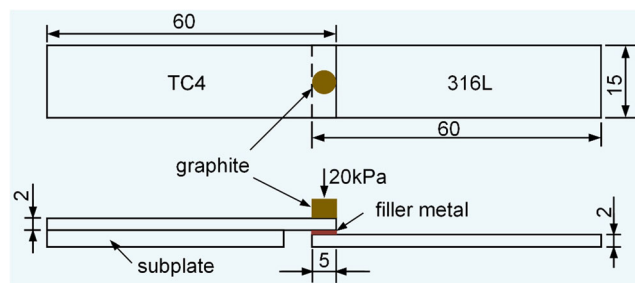
#### 3.1 Ti-25Zr-50Cu amorphous filler metal

Figure 4a shows the X-ray diffraction pattern of the filler metal. It can be seen that no sharp diffraction peaks corresponding to crystalline phases are observed, indicating that the filler metal is with amorphous structure. In addition, the backscattered electron image in Fig. 4b further shows that the filler metal is homogeneous. The phase transition temperature is obtained by calculating the inflection point of baseline of DTA curve. As shown in Fig. 5, the glass transition temperature ( $T_g$ ) of the amorphous filler metal was determined to be about 370 °C and the crystallization temperature ( $T_x$ ) to be about 412 °C. When the brazing temperature reached  $T_g$ , amorphous filler metal began to transform into crystallization with structural relaxation, and this transformation finished at  $T_x$ . As similar as  $T_g$  and  $T_x$ , the melting temperature ( $T_m$ ) (also called solidus temperature,  $T_s$ ) and liquidus temperature ( $T_l$ ) of the amorphous filler metal were calculated to be 837 and 860 °C, respectively.

#### 3.2 Effect of brazing time on the interfacial microstructure and mechanical property of joint

##### 3.2.1 Microstructure

Figure 6 illustrates the interfacial morphology of TC4 titanium alloy/316L stainless steel joints brazed at 910 °C for different brazing time. The brazed seams primarily consisted of three



**Fig. 2** Assembly of brazed samples

distinctive regions (marked as 1, 2, and 3) and had similar interfacial morphology under different brazing time. Generally speaking, high temperatures are favorable for rapid diffusion of solutes between filler metal and base metals during brazing process. Consequently, the thickness of brazed seams increased slightly from 64 to 76 μm with the increase of brazing time. Especially, the thickness of region 1 increased with the increase of brazing time.

The typical joint brazed at 910 °C/10 min was mainly examined by EPMA to analyze the constituent of different regions, and the results are listed in Table 2. Region 1 was a diffusion layer with the constituents of about 73% Ti, 7% Cu, 4% Fe, and 10% Al in atom percent (location A). According to Ti-Cu [22] and Ti-Cu-Fe [23] phase diagrams, the phase at location A was confirmed to be β-Ti. During brazing, under the concentration gradient, Ti atoms diffused into the molten filler metal from TC4 titanium substrate with a dilution of Ti in β-Ti region. Meanwhile, a few Cu and Fe atoms diffused into this region. As β-Ti stabilizers, V, Cu, and Fe could promote the formation of β-Ti phase. Needle-like Widmanstätten microstructure formed adjacent to TC4 titanium substrate in region 1. The Widmanstätten is essentially (α+β)-Ti phase transformed from high-temperature β-Ti, which was also observed in the research of brazing TC4 titanium alloy with

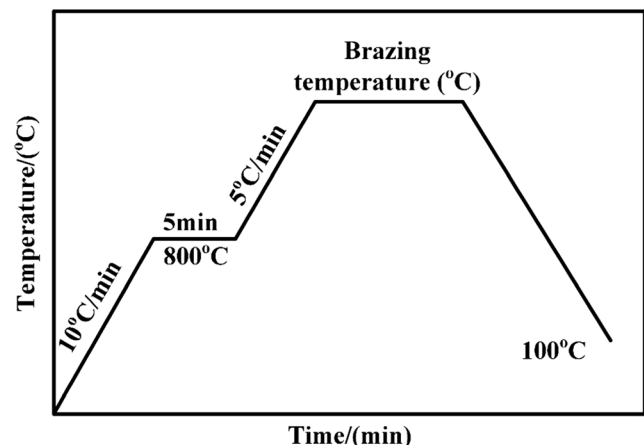
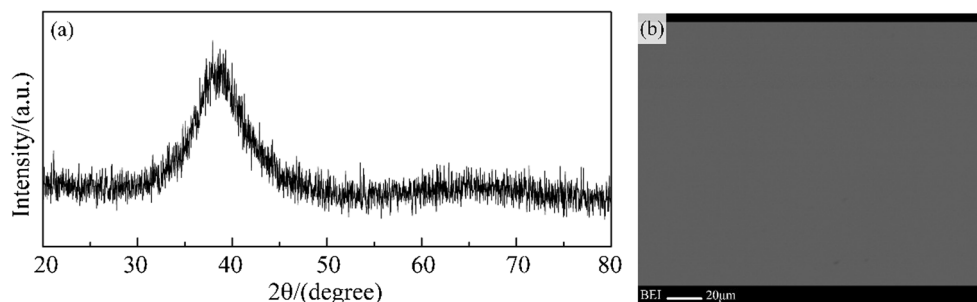


**Fig. 3** Schematic of the heating curve during brazing process

**Fig. 4** **a** X-ray diffraction pattern and **b** backscattered electron image of the filler metal



the same Ti-based filler metal [24]. Increasing the brazing time could promote the Widmanstätten transformation [25]; consequently, the amount of Widmanstätten microstructure increased. In addition, two distinctive reaction phases formed at location E, in which the Cu content was higher than that in  $\beta$ -Ti. Based on the EPMA quantitative analysis results, the phases at location E were composed of  $\beta$ -Ti and an acicular microstructure as marked by arrow in Fig. 6d, which was  $\text{Ti}_2\text{Cu}$  according to Ti-Cu-Fe ternary phase diagram. In our previous research [26], TC4 alloy/316L stainless steel was brazed with Ti-43.75Cu-6.25Zr-6.25Ni-6.25 V (at%) amorphous filler metal, which had more Ti and less Cu compared with Ti-25Zr-50Cu filler metal in this paper. However, more  $\text{Ti}_2\text{Cu}$  phase precipitated in the front of  $\beta$ -Ti region, particularly at 900 °C/15 min, indicating the restriction of Cu diffusion from filler metal to TC4 substrate in this research.

White gray phase (location B) and eutectic microstructure were formed in region 2, and the eutectic microstructure was also detected in other literatures [15, 24]. Higher magnification image of eutectic microstructure is shown in Fig. 6d (location F). According to Table 2, Ti, Zr, and Cu were the major elements at location B with the constituent of 38% Ti + 25% Cu + 16% Zr in atom percent. Due to the mutual diffusion between molten filler metal and base metals, Ti content at location B was lower than that of the initial filler metal. According to Cu-Ti-Zr ternary phase diagram [27], the white gray phase (location B) was concluded to be  $\alpha$ -Ti +  $\lambda$ - $\text{Cu}_2\text{TiZr}$ . The ratio of the

stoichiometric coefficients of Ti and Cu of the phase at location F was approximately 2:1; therefore, this phase was possibly  $\text{Ti}_2\text{Cu}$ . In addition, the region 2 mainly consisted of Ti, Zr, and Cu, which was likely because the region 2 is retained from the molten filler metal.

In region 3, according to EPMA quantitative analysis results, the phase at location C was a kind of Ti-Cu-Fe phase composed of complicated Ti-Cu and Ti-Fe intermetallic compounds. In Fig. 7, it could be seen that Ti content in region 3 was higher than that in region 2, which was mainly attributed to the strong reactivity between Ti and Fe. This continuous Ti-Cu-Fe reaction layer was also detected in the joints brazed with Ag-based filler metal [28]. It could be seen from Fig. 6f that Ti content decreased gradually from TC4 titanium substrate side to the eutectic structure in region 2, forming a trough in this region, then increased in region 3. The formation of  $\text{Ti}_2\text{Cu}$  consumed large Ti atoms in region 2; thus, Ti trough presented in white gray phase. The variation of Ti content displayed in line scanning results was consistent with the mapping analysis results in Fig. 7. In addition, more eutectic microstructure and Ti-Cu-Fe phase formed in our previous study [26], which indicated that the metallurgical reaction within the joint accelerated likely because of the higher mixing enthalpy with the addition of V and Ni in filler metal.

It was noteworthy that a thin reaction layer generated close to 316L stainless steel substrate with the segregation of a large amount of Cr as pointed out by the arrow in Fig. 6f. The trace of Cr segregation was demonstrated by the mapping distribution of Cr in Fig. 7. The reaction layer of Cr segregation with thickness of about 5  $\mu\text{m}$  could be easily etched by Kroll reagent, as shown by dotted lines in Fig. 6e. According to the elemental composition in Table 2 (location D), this reaction layer was suggested to be the mixture of Fe solid solution ( $\text{Fe}_{\text{ss}}$ ) and  $\sigma$ -phase.

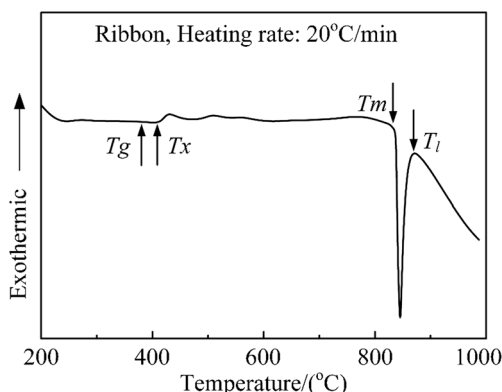
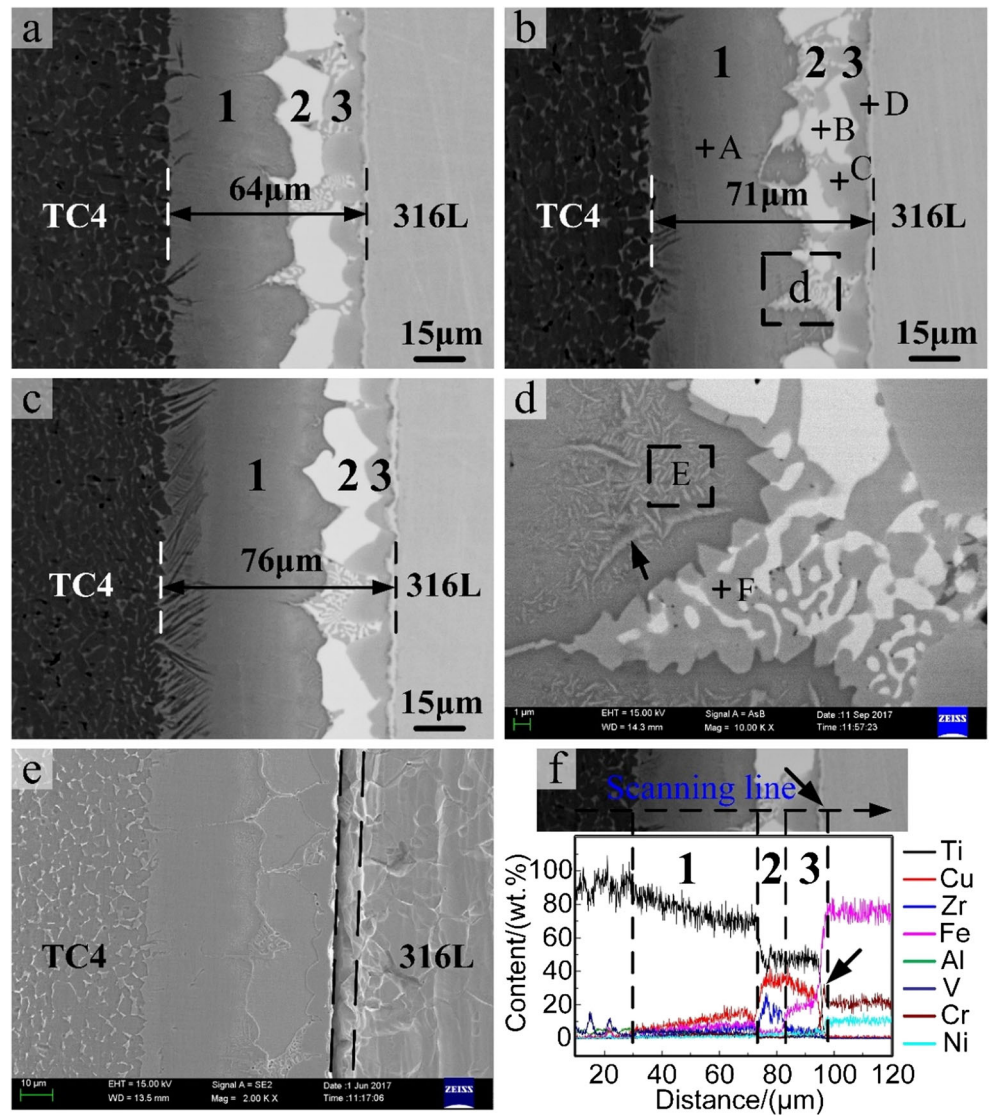


**Fig. 5** DTA curve of Ti-25Zr-50Cu amorphous filler metal

### 3.2.2 Mechanical property

The variation of brazing time will lead to changes in microstructure, which would eventually affect the mechanical

**Fig. 6** Backscattered electron images (BEI) of brazed joints at 910 °C for different brazing time: **a** 5 min, **b** 10 min, **c** 15 min; **d** high magnification image of the square area in **b**; **e** secondary electron image (SEI); **f** line scanning results of the joint brazed at 910 °C/10 min



properties of the brazed joints. Figure 8 shows the average shear strength and typical tensile-shear displacement-strain curves of the joints brazed for different brazing time at 910 °C. The shear strength of the joints first increased and then decreased with the increase of brazing time, and the peak value of 47 MPa (Fig. 8a) was obtained under the brazing time

of 10 min within the 910 °C group. It is well known that the displacement of the brazed joints can represent the elongation qualitatively. The variation of the joint elongation was consistent with that of the joint shear strength. Thus the optimized brazing time was determined to be 10 min within the 910 °C group. The reason of change for mechanical properties of

**Table 2** EPMA quantitative analysis results of the locations in Fig. 6

Location	Percent of elements (at%)								Possible phases
	Ti	Cu	Fe	Zr	Al	V	Ni	Cr	
A	73.4	6.8	4.4	0.9	8.7	1.1	0.5	1.5	β-Ti
B	37.9	24.5	8.1	16.3	7.5	0.7	1.3	2.2	α-Ti + λ-Cu <sub>2</sub> TiZr
C	50.1	24.1	16.2	2.8	2.1	0.5	0.7	2.1	Ti-Cu-Fe
D	6.0	0.6	61.7	–	0.3	–	–	30.7	σ-phase + Fe <sub>ss</sub>
E	67.8	12.0	6.8	3.6	4.6	0.5	1.0	1.9	Ti <sub>2</sub> Cu + β-Ti
F	61.6	29.8	1.8	3.0	1.0	1.4	1.2	0.2	Ti <sub>2</sub> Cu

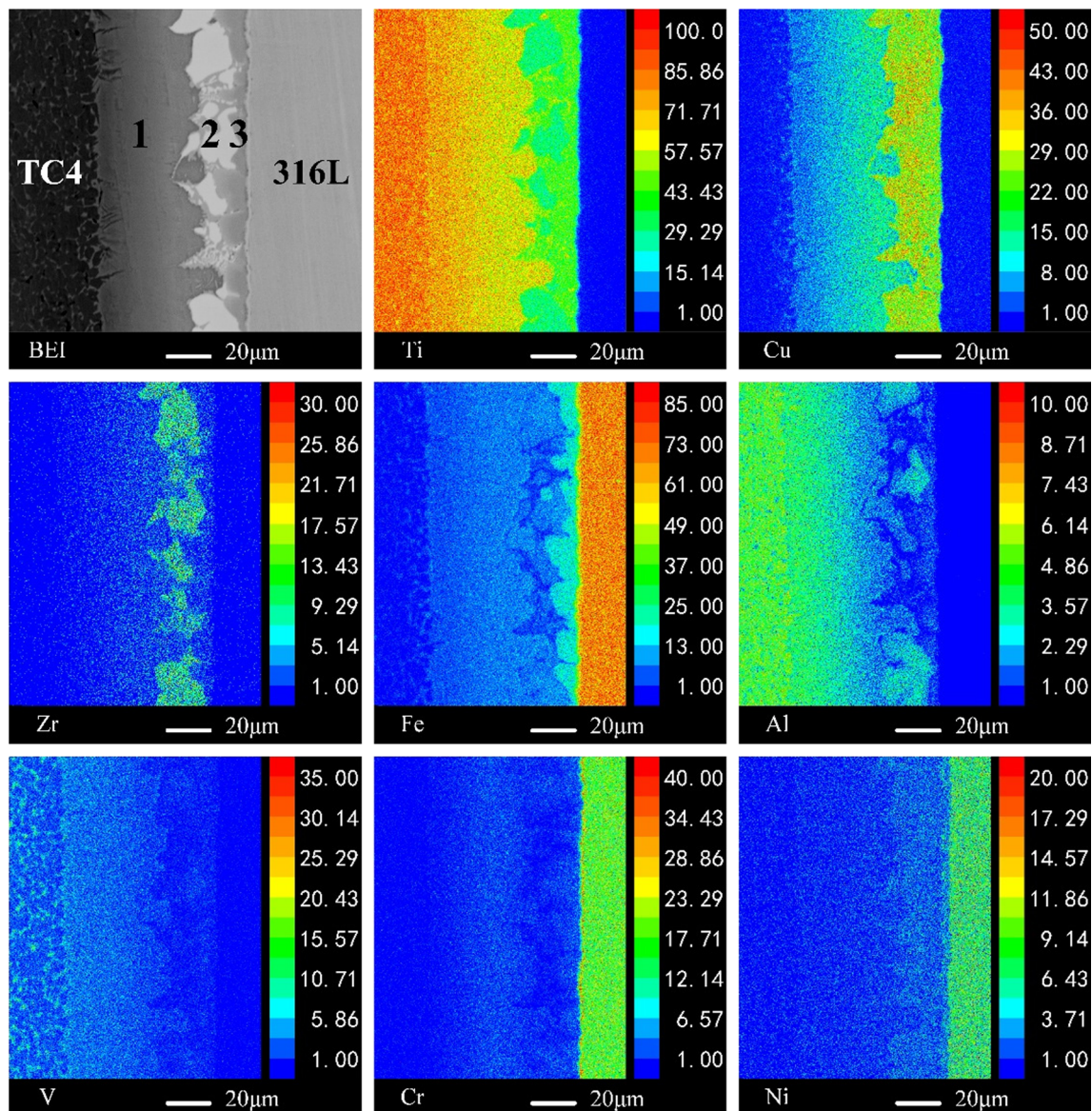


Fig. 7 EPMA mapping analysis results of joint brazed at 910 °C/10 min

joints is likely because of the variation of interface microstructure, which would be discussed in following section.

### 3.3 Effect of brazing temperature on the interfacial microstructure and mechanical properties of joint

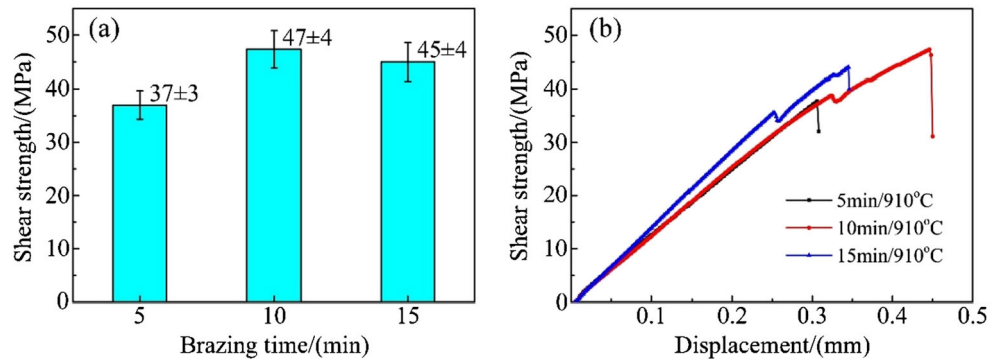
#### 3.3.1 Microstructure

The interfacial morphology of joints brazed at different temperatures is shown in Fig. 9. It could be seen that the microstructure of brazed joints at different brazing temperatures was similar to that for different brazing time. The thickness of brazed seam ( $\sim 70 \mu\text{m}$ ) had no obvious change from 890 to 930 °C; however, it reached 86  $\mu\text{m}$  at 950 °C, which was mainly attributed to the transformation of large

amount of acicular ( $\alpha+\beta$ )-Ti phases (Widmanstätten). The distribution and morphology of reaction phases in region 2 changed significantly at different brazing temperatures. Particularly, the formation of eutectic  $\text{Ti}_2\text{Cu}$  phase was restrained, and the Ti-Cu-Fe phase, close to 316L substrate, increased due to the accelerated interdiffusion. The variation of region 2 also resulted in widening of region 1 due to the Cu diffusion from filler metal to this region; thus, the formation of  $\beta$ -Ti phase was promoted.

From the line scanning result marked by arrow in Fig. 9e and the distribution of Cr in Fig. 10, the segregation of Cr was also detected close to 316L stainless steel substrate, indicating the formation of  $\sigma$ -phase. The formation of  $\sigma$ -phase could be observed in all joints at different brazing temperatures, particularly at 950 °C, as shown in

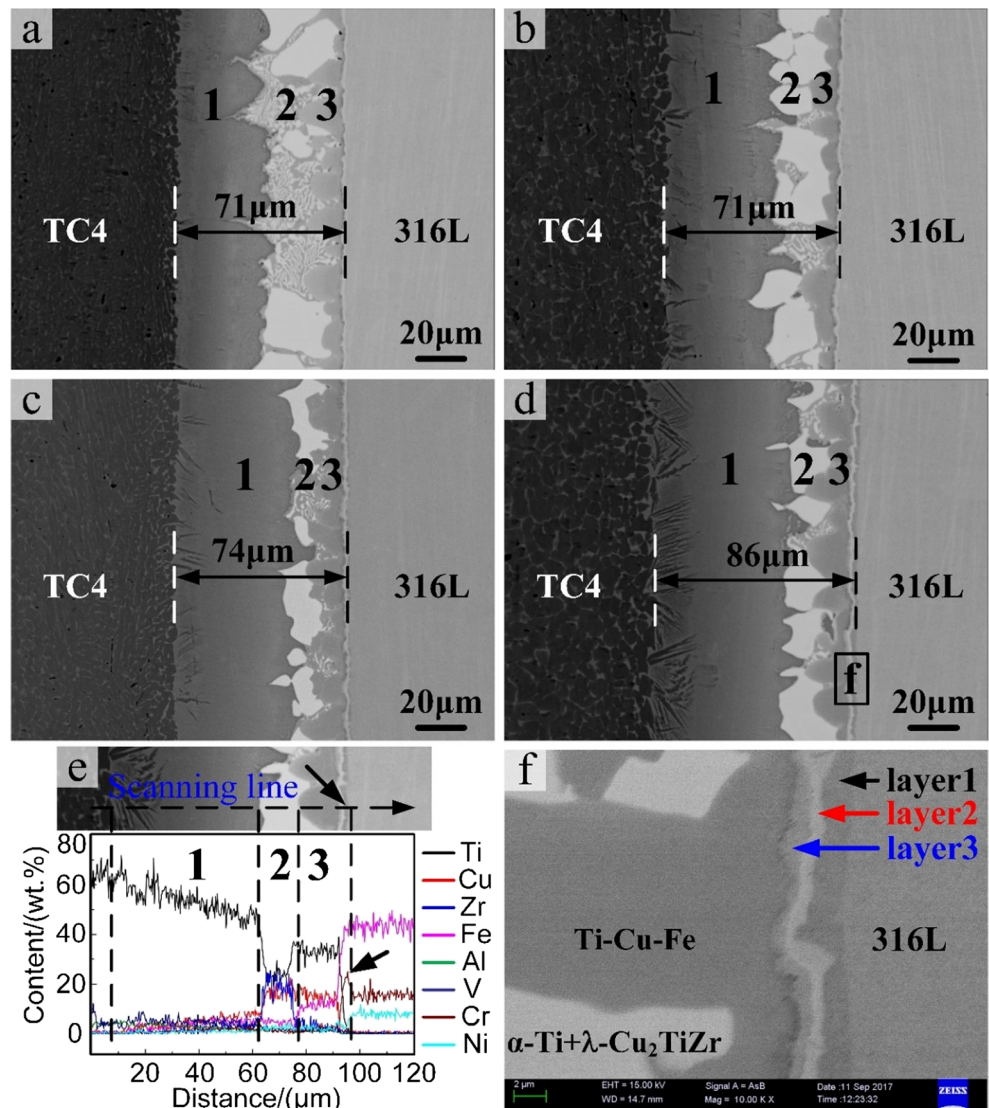
**Fig. 8** **a** Average shear strength of the brazed joints; **b** typical tensile-shear displacement-strain curves of joints brazed at 910 °C for different brazing time



**Fig. 9d.** The reaction layer of  $\sigma$ -phase contained 58 at% Fe and 31 at% Cr at 950 °C. Generally, when Cr content ranges from about 45 to 50 (at%),  $\sigma$ -phase would be precipitated in Cr-Fe alloy according to Cr-Fe binary diagram [29]. However, due to the effect of elemental segregation, the  $\sigma$ -phase could be precipitated at lower Cr content

within austenitic stainless steels [30] as well as the formation of Fe solid solution ( $Fe_{ss}$ ). Virtually,  $\sigma$ -phase is an intermetallic phase and prone to precipitate along the grain and cell boundaries [31]. The formation of  $\sigma$ -phase would not only deteriorate the mechanical properties by causing local embrittlement, but also reduce the corrosion

**Fig. 9** Backscattered electron images of joints brazed for 10 min at different brazing temperatures: **a** 890 °C, **b** 910 °C, **c** 930 °C, **d** 950 °C; **e** line scanning results of the joint brazed at 950 °C/10 min; **f** high magnification image of the square area in **d**



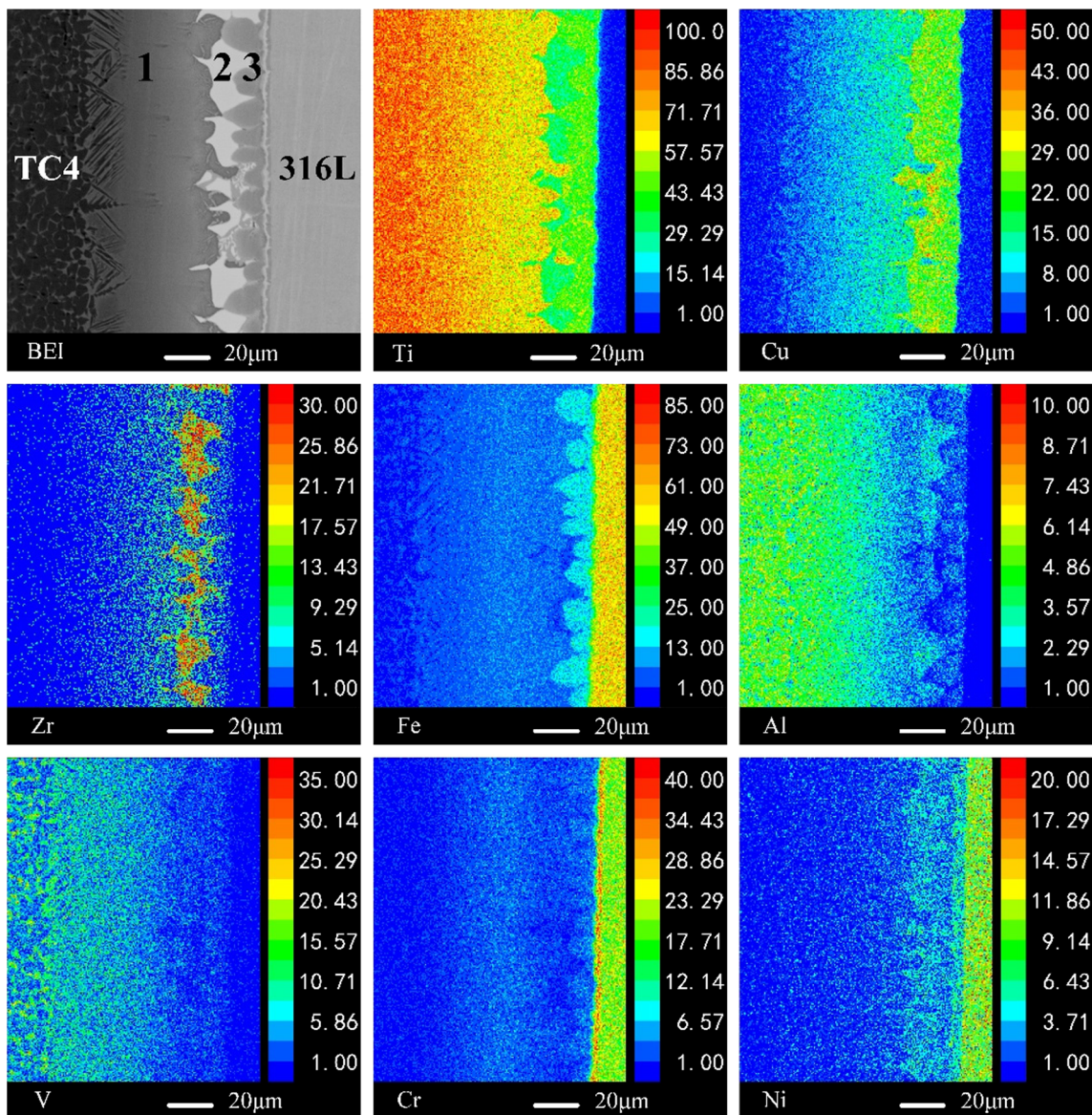


**Fig. 10** EPMA mapping analysis results of the joint brazed at 950 °C/10 min

resistance of stainless steel. In Fig. 6e, the corrosion behavior of  $\sigma$ -phase was mainly caused by the chromium depletion due to the precipitation of chromium carbide at grain boundaries [32]. The formation of  $\sigma$ -phase was also detected in the research of Ti (Gr.2)/UNS S31254 with Ti-Zr-Ni-Cu-Be amorphous filler alloy, and the joints fractured along the reaction layer of  $\sigma$ -phase [18]. Therefore, in this research, the site where  $\sigma$ -phase formed was believed to be the weak part of brazed joints.

According to above analysis, it was essential to investigate the site where  $\sigma$ -phase formed. The high magnification image of the  $\sigma$ -phase +  $\text{Fe}_{\text{ss}}$  layer was further obtained as shown in Fig. 9f, and three distinctive reaction layers (layers 1, 2, and 3) were exhibited adjacent to 316L stainless steel substrate. Among the three layers, layer 1

was  $\sigma$ -phase +  $\text{Fe}_{\text{ss}}$  with a large amount of Cr segregation here, which could be demonstrated by the elemental distribution (Fig. 9e and Fig. 10). Whereas the total thickness ( $< 2 \mu\text{m}$ ) of layer 2 and layer 3 was too small to be detected by EPMA and SEM. However, according to ref. [28], layer 2 and layer 3 were suggested to be Ti-Fe or Ti-Fe-Cr phase. Moreover, considering the elemental line scanning results around the interface of brazed seam/316L stainless steel substrate, layer 2 was Ti-Fe-Cr phase and layer 3 was Ti-Fe phase. Ti-Cu-Fe phase in region 3 was generated from solidification, while the mutual diffusion contributed to the formation of Ti-Fe phase, i.e., the formation of Ti-Fe phase was a solid state transformation. So the interface of Ti-Cu-Fe phase/Ti-Fe phase was an essential interface of solid/liquid during



solidification. It was believed that stress concentration easily formed along this interface, which would be the main factor to fail the brazed joints. So the interface of Ti-Cu-Fe layer/Ti-Fe layer was regarded as the weakest part of joints.

### 3.3.2 Mechanical property

As shown in Fig. 11a, with the increase of brazing temperature, the average shear strength of the joints increased gradually. The maximum shear strength of 65 MPa was obtained at 950 °C for 10 min. As mentioned previously, the higher brazing temperature could accelerate the diffusion of molten filler metal, so the thickness of region 2 (residual filler metal) gradually reduced. It seems that the shear strength of joints increased with the decrease of thickness of region 2, while the change of thickness of the entire joint could not affect the shear strength directly, which was already proved in above. In Fig. 11b, it could also be seen that the displacement and elongation of joints first increased and then decreased with increasing the brazing temperature. The elongation reached the peak value at 930 °C. In terms of the comprehensive mechanical properties, the optimized brazing temperature was between 930 and 950 °C. In our previous research [26], the maximum shear strength of the joints brazed at different brazing temperatures (900–990 °C) reached 65 MPa, same to that in this research. Nevertheless, the variation range of brazing temperature was smaller in this research, which was meaningful for brazing of TC4 alloy/316L stainless steel. In addition, compared with the brazing time, the brazing temperature had greater effect on the mechanical properties of joints.

### 3.4 Fracture analysis

In this research, all joints had similar fracture path and morphology. Figure 12 illustrates the typical fracture morphology and path of the joints brazed at 910 °C/10 min and 950 °C/10 min after shear test. The corresponding EDS

analysis results of fracture surfaces are listed in Table 3 and Table 4. The joints fractured at the interface of brazed seam/316L stainless steel substrate. Meanwhile, a large amount of secondary cracks spread throughout the cross section of the brazed joint, as pointed out by the arrows in Fig. 12a, d. In Fig. 12b, c, the abruption could be clearly seen on both TC4 titanium alloy and 316L stainless steel sides marked by the yellow dotted line. The abruption was mainly caused by the natural brittleness and incoherent crystal structure between the reaction phases (locations E1 and F1, Table 3). After shear test, a large amount of cleavage facets, marked by the dotted rectangle in Fig. 12b, c, were found with transgranular fracture feature. Various reaction phases were observed, including  $(\text{Fe, Cr})_2\text{Ti}$ , TiFe, Ti-Cu-Fe,  $\alpha\text{-Ti} + \lambda\text{-Cu}_2\text{TiZr}$ , and  $\sigma\text{-phase} + \text{Fe}_{\text{ss}}$ . Among them,  $(\text{Fe, Cr})_2\text{Ti}$  was a kind of Laves phase with the composition of  $\text{AB}_2$  [33]. The abruption and cleavage facets were also found on the fracture surface of the joint brazed at 950 °C/10 min. In addition, the similar reaction phases (Table 4) with 910 °C/10 min were detected. It was noteworthy that the cellular surfaces (Fig. 12f) presented on 316L side of fracture surfaces, indicating the intergranular fracture feature. Based on above analysis and interfacial microstructure of joints, it was further confirmed that, during shear test, the cracks initiated at the interface of Ti-Cu-Fe layer/TiFe layer with both transgranular and intergranular fracture feature. Subsequently, the cracks spread along the interface of brazed seam/316L stainless steel substrate with the formation of a large amount of cleavage facets on the fracture surfaces.

In order to further investigate the reaction phases, XRD test of the fracture surfaces was carried out, and the typical XRD patterns are illustrated in Fig. 13. Besides the major 316L matrix (austenite, Cr-Ni-Fe-C phase),  $\sigma$ -phase (Fe-Cr) and Ti-Fe-Cu ( $\text{Cu}_{0.8}\text{Fe}_{0.2}\text{Ti}$ ) were detected on 316L stainless steel side. Moreover, additional  $\text{Cr}_{13}\text{Fe}_{35}\text{Ni}_3\text{Ti}_7$  (Ti-Fe-Cr) phase was also identified, which was not detected previously possibly due to its small amount. Furthermore, a large amount of Ti-based intermetallic compounds were detected on TC4 substrate side, including

**Fig. 11** **a** Average shear strength of joints; **b** typical tensile-shear displacement-strain curves of joints brazed at different brazing temperatures for 10 min

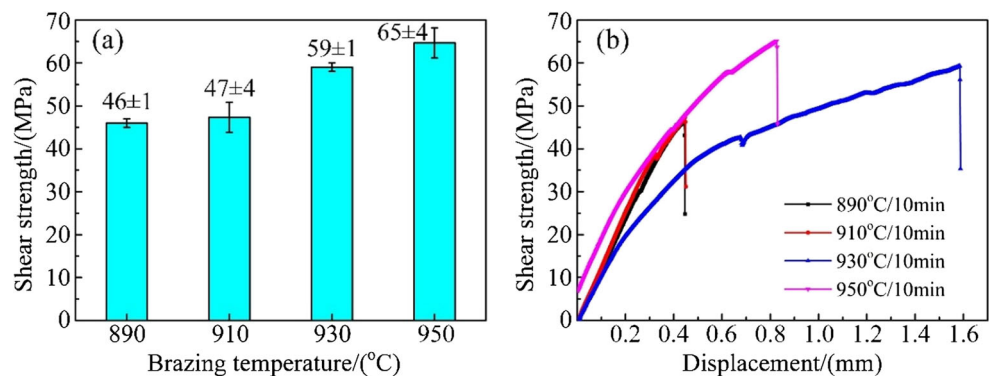
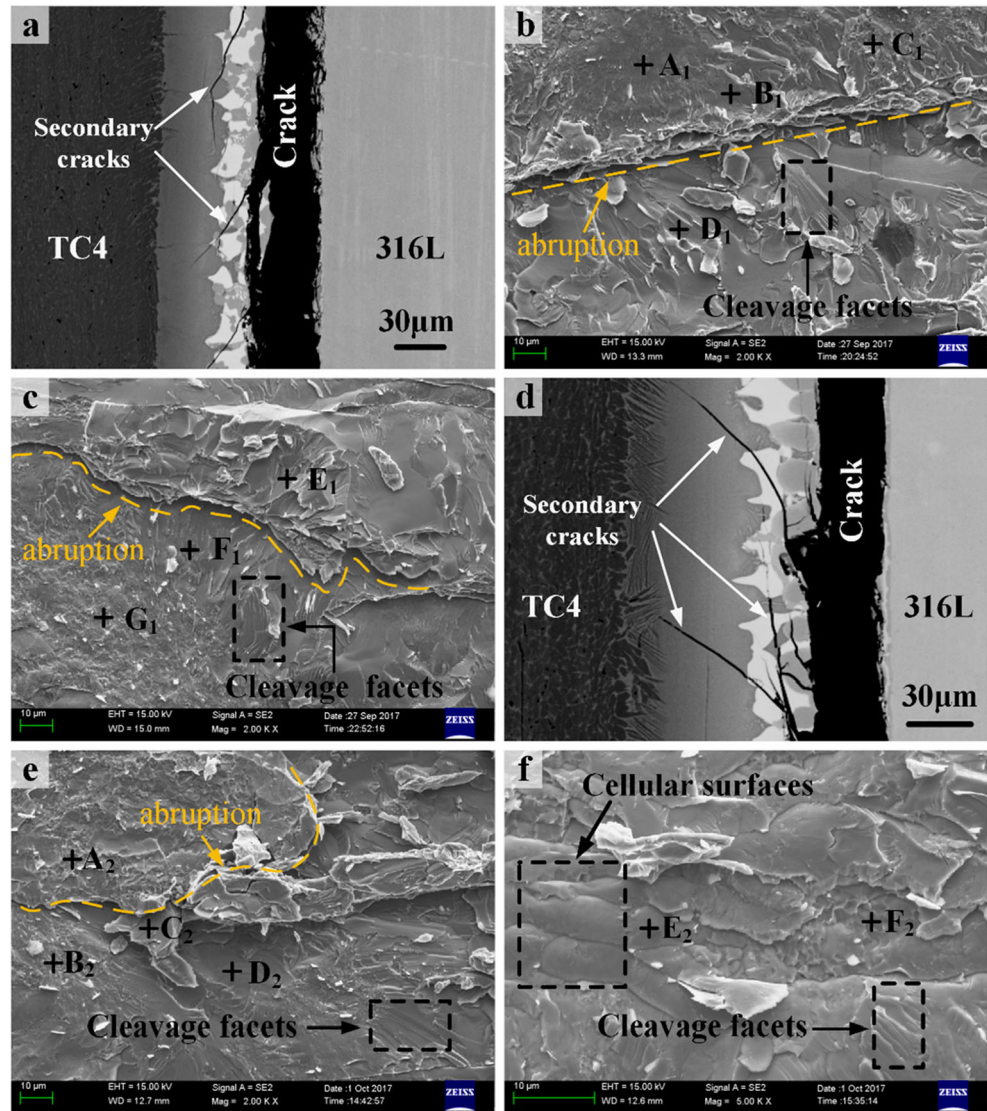


**Fig. 12** **a** Fracture path and the morphology of the fracture surface of **b** TC4 titanium alloy side and **c** 316L stainless steel side at 910 °C/10 min; **d** fracture path and the morphology of the fracture surface of **e** TC4 titanium alloy side and **f** 316L stainless steel side at 950 °C/10 min



$\text{Fe}_2\text{Ti}$ ,  $\text{Ti-Fe-Cu}$  ( $\text{Cu}_{0.8}\text{Fe}_{0.2}\text{Ti}$ ), and  $\text{Ti}_2\text{Cu}$  phases. Among them,  $\text{Ti-Fe-Cu}$  phase was the major reaction phase on TC4 titanium alloy side. The detection of  $\text{Ti-Fe-Cu}$  phases,  $\sigma$ -phase,  $\text{TiFe}$ , and  $\text{Cr}_{13}\text{Fe}_{35}\text{Ni}_3\text{Ti}_7$  was consistent with the above analysis.

### 3.5 Interface of brazed seam/316L stainless steel

Since the joints failed at the interface of brazed seam/316L stainless steel substrate, the transition zone between brazed seam and 316L stainless steel substrate was further

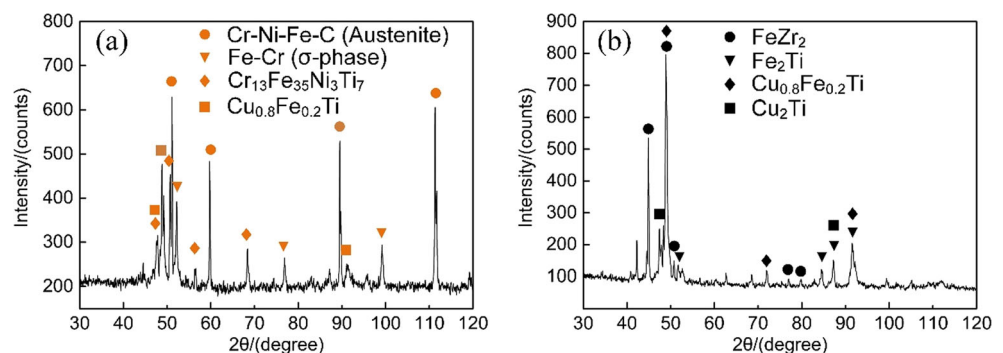
**Table 3** EDS analysis results of the locations in Fig. 12 (910 °C/10 min)

Location	Percent of elements (at%)								Possible phases
	Ti	Cu	Fe	Zr	Al	V	Ni	Cr	
A <sub>1</sub>	32.1	1.5	49.6	2.0	4.3	0.9	2.7	11.0	(Fe, Cr) <sub>2</sub> Ti
B <sub>1</sub>	43.4	3.4	40.2	1.7	1.5	0.7	3.3	6.9	TiFe
C <sub>1</sub>	47.4	23.5	17.3	2.7	3.9	0.7	2.1	2.3	Ti-Cu-Fe
D <sub>1</sub>	33.9	24.6	8.9	17.8	8.5	1.7	2.0	2.6	$\alpha$ -Ti + $\lambda$ -Cu <sub>2</sub> TiZr
E <sub>1</sub>	34.1	25.8	8.6	17.2	8.1	1.8	2.1	2.4	$\alpha$ -Ti + $\lambda$ -Cu <sub>2</sub> TiZr
F <sub>1</sub>	42.3	24.5	20.6	2.3	3.0	0.8	4.2	2.4	Ti-Cu-Fe
G <sub>1</sub>	3.2	0.5	65.0	0.6	0.9	0.8	3.6	25.4	$\sigma$ -phase + Fe <sub>ss</sub>

**Table 4** EDS analysis results of the locations in Fig. 12 (950 °C/10 min)

Location	Percent of elements (at%)								Possible phases
	Ti	Cu	Fe	Zr	Al	V	Ni	Cr	
A <sub>2</sub>	9.5	0.4	59.8	0.4	0.4	0.6	3.4	25.4	$\sigma$ -phase + Fe <sub>ss</sub>
B <sub>2</sub>	29.5	0.2	53.0	1.3	0.7	0.5	5.1	9.8	(Fe, Cr) <sub>2</sub> Ti
C <sub>2</sub>	34.3	2.6	46.8	2.1	1.3	0.5	4.5	7.9	TiFe
D <sub>2</sub>	45.8	21.0	19.5	1.8	5.0	1.1	3.2	2.7	Ti-Cu-Fe
E <sub>2</sub>	36.8	32.4	18.6	2.1	3.7	0.6	2.1	4.3	Ti-Cu-Fe
F <sub>2</sub>	1.1	0.4	66.3	0.1	0.3	0.6	3.3	28.0	$\sigma$ -phase + Fe <sub>ss</sub>

investigated. Figure 14 illustrates the evolution of this transition zone at different brazing time and temperature. And the transition zone was composed of TiFe, (Fe, Cr)<sub>2</sub>Ti, and  $\sigma$ -phase + Fe<sub>ss</sub>. The layer numbers in Fig. 14f were corresponding to those in Fig. 9f. It could be seen in Fig. 14 that the morphology of transition zone almost had no change with the increase of brazing time, indicating its insensitivity to the brazing time, which was similar to the results in our previous research [26]. Consequently, the brazing time had little effect on the variation of mechanical properties of brazed joints. And the trace of  $\sigma$ -phase + Fe<sub>ss</sub> could be found in the area close to 316L stainless steel substrate. However, increasing brazing temperature had promoted the growth of  $\sigma$ -phase + Fe<sub>ss</sub> layer. This reaction layer could not be seen at 890 °C, but the distribution of  $\sigma$ -phase + Fe<sub>ss</sub> layer changed from discontinuous to continuous feature with the increase of brazing temperature. In addition, the total thickness of TiFe and (Fe, Cr)<sub>2</sub>Ti layers also increased. Generally, the thickness of IMC layers less than 3–5  $\mu$ m was considered appropriate [34, 35]. Thicker IMC layers indicated the sufficient mutual diffusion between filler metal and base metals. So wider interface would benefit the shear strength of joints. However, the excessive growth of transition zone might deteriorate the ductility and reduce the elongation of joints. This was consistent with the above analysis on the variation of joint mechanical properties.

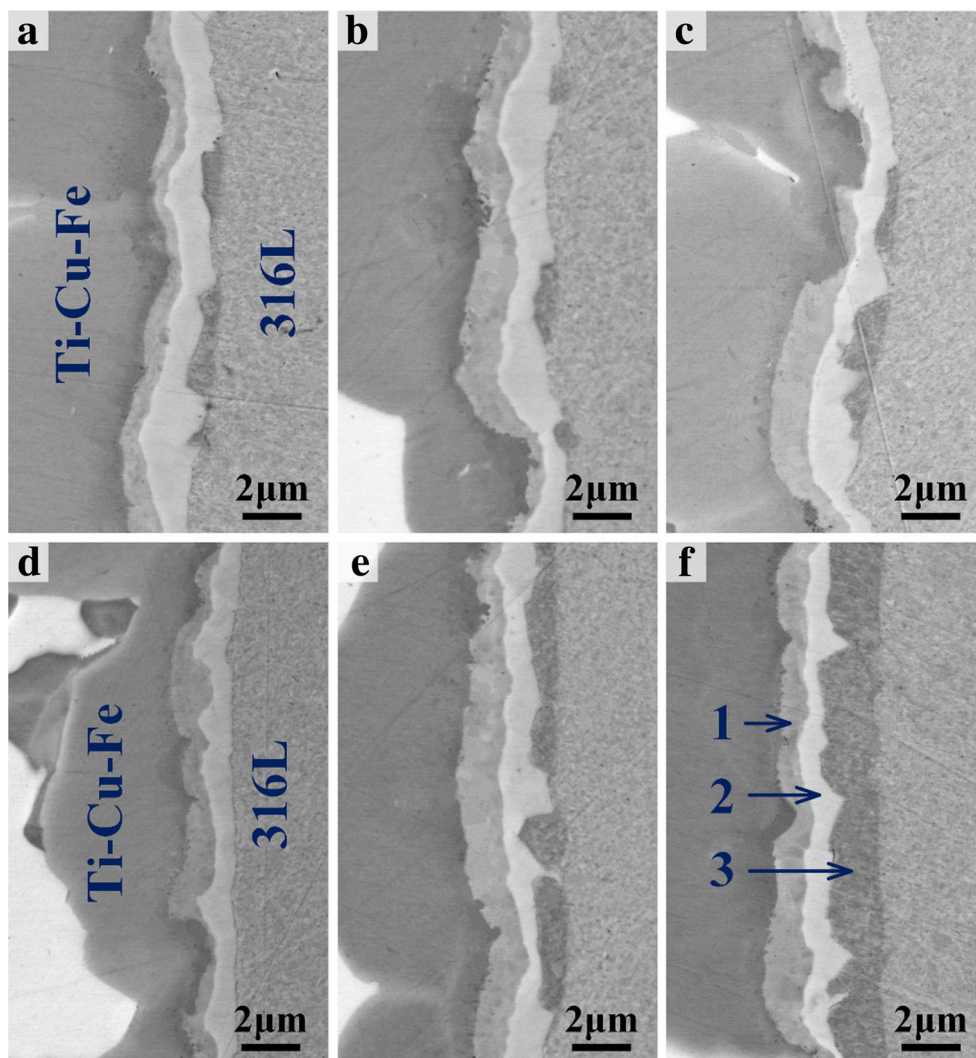
**Fig. 13** XRD patterns of fracture surfaces at 950 °C/10 min on **a** 316L stainless steel side and **b** TC4 titanium alloy side

According to the EDS results (Tables 3 and 4), the B<sub>2</sub> and A<sub>1</sub> phases were possibly Ti-Fe-Cr phase ((Fe, Cr)<sub>2</sub>Ti); meanwhile, TiFe phase was also detected (locations B<sub>1</sub> and C<sub>2</sub>) on the fracture surfaces. The Ti-Fe-Cr and Ti-Fe reaction phases could not be detected in the brazed seam due to their tiny dimension. However, after shear test, a larger fracture surface containing these two reaction phases was present, thus the reaction phases could be easily identified. A large amount of Ti atoms were driven to diffuse from molten filler metal and TC4 titanium substrate toward 316L stainless steel substrate under the concentration gradient of Ti. The consumption of filler metal contributed to the growth of TiFe and (Fe, Cr)<sub>2</sub>Ti reaction layers. Higher brazing temperature promoted the atomic diffusion and led to a larger thickness of TiFe and (Fe, Cr)<sub>2</sub>Ti layers. Subsequently, these two reaction layers would prevent the components of 316L substrate from diffusing into the brazed seam, thus a large amount of chromium atoms segregated here. So higher temperature also promoted the growth of  $\sigma$ -phase + Fe<sub>ss</sub> layer. According to the above analysis, the interfacial microstructure of TC4 titanium alloy/Ti-25Zr-50Cu/316L stainless steel joint was further confirmed to be TC4 titanium substrate/Widmanstätten/ $\beta$ -Ti + Ti<sub>2</sub>Cu/( $\alpha$ -Ti +  $\lambda$ -Cu<sub>2</sub>TiZr) + Ti<sub>2</sub>Cu/Ti-Fe-Cu/TiFe/(Fe, Cr)<sub>2</sub>Ti/ $\sigma$ -phase + Fe<sub>ss</sub>/316L stainless steel substrate.

### 3.6 Microstructure evolution mechanism

A schematic diagram in Fig. 15 was proposed to evaluate the microstructure evolution and phase formation mechanism of the joints. The sample assembly is exhibited in Fig. 15a. When the brazing temperature reached the melting temperature ( $T_m$ ) of amorphous filler metal, the filler metal began to melt. While the brazing temperature reached the liquids temperature ( $T_l$ ) of filler metal, the filler metal melted completely. Meanwhile, two base metals had dissolved by some amount, which led to the formation of two solid/liquid interfaces, i.e., the interfaces of TC4 titanium substrate/molten filler metal and molten filler metal/316L stainless steel substrate. Atomic mutual

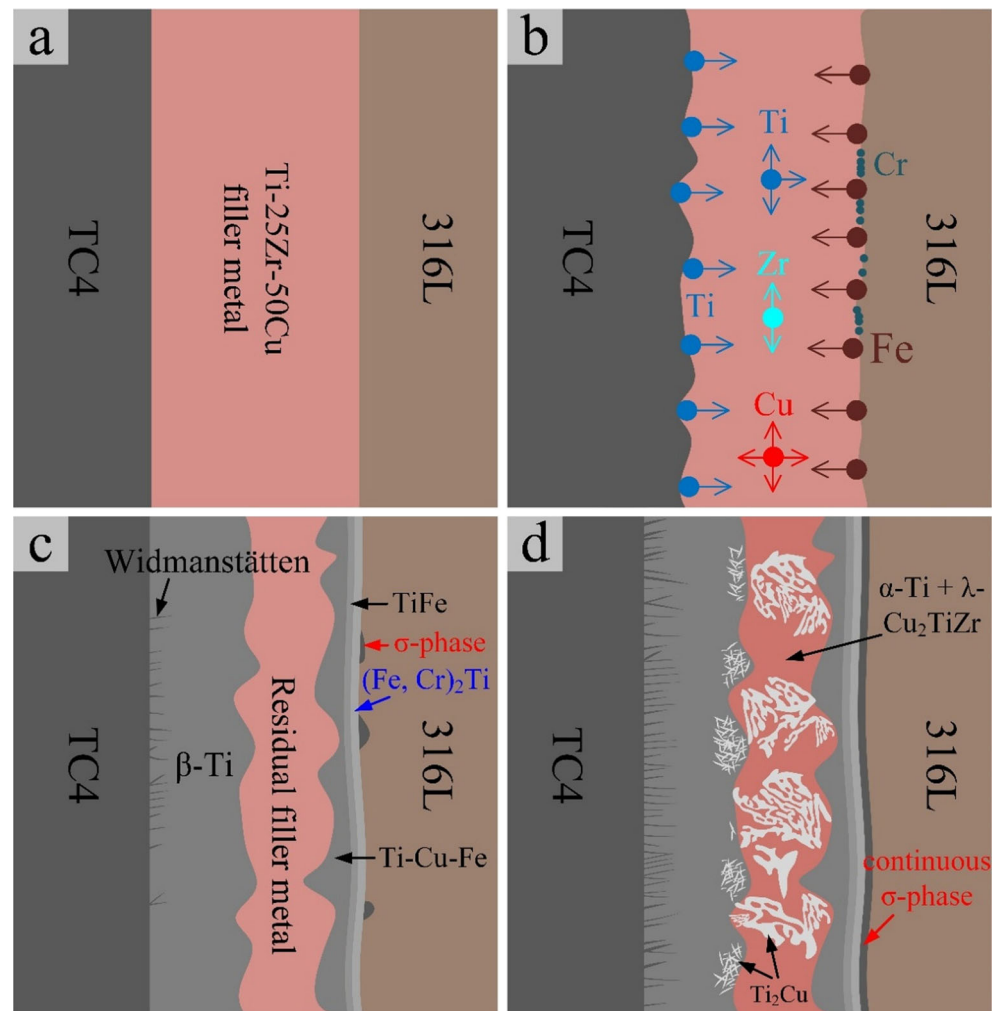
**Fig. 14** Microstructure morphology of the brazed seam/316L interface (TiFe/(Fe, Cr)<sub>2</sub>Ti/ $\sigma$ -phase + Fe<sub>ss</sub>) at different brazing parameters: **a** 910 °C/5 min, **b** 910 °C/10 min, **c** 910 °C/15 min, **d** 890 °C/10 min, **e** 930 °C/10 min, **f** 950 °C/10 min



diffusion between filler metal and base metals occurred during brazing. Figure 15b shows that different atoms diffuse toward different orientations, which was mainly dominated by the concentration gradient and reaction capacity of different atoms in the joint. A large amount of Cr atoms segregated in the brazed seam adjacent to 316L stainless steel. At elevated temperature in Fig. 15c, different reaction phases would be first formed in other regions except for the region of residual filler metal where eutectic reaction occurred during solidification. TiFe and (Fe, Cr)<sub>2</sub>Ti phases generated close to 316L stainless steel substrate, which resulted from the atomic diffusion with the presentation of smooth interface of (Fe, Cr)<sub>2</sub>Ti layer/TiFe layer. In fact, the interface of solid/liquid was proved to be that of Ti-Cu-Fe layer/TiFe layer. Moreover, discontinuous  $\sigma$ -phase + Fe<sub>ss</sub> formed adjacent to 316L stainless steel substrate. On TC4 titanium alloy side, the diffusion layer of  $\beta$ -Ti formed under the influence of  $\beta$ -Ti stabilizers; subsequently, Widmanstätten structure precipitated from elevated-

temperature  $\beta$ -Ti. With the temperature decreasing during solidification, as shown in Fig. 15d, the amount of Widmanstätten became larger due to its sufficient growth. During brazing, a few amount of Cu atoms diffused into  $\beta$ -Ti region, and then Ti<sub>2</sub>Cu precipitated in front of  $\beta$ -Ti region toward the residual filler metal region, which was attributed to the saturation concentration of Cu in  $\beta$ -Ti. In the region of residual filler metal, Ti<sub>2</sub>Cu was first generated with eutectic reaction and consumption of some amount of Ti atoms, and then the residual filler metal transformed into  $\alpha$ -Ti + Cu<sub>2</sub>TiZr in the middle part of joint. In addition, it was notable that the reaction layer of  $\sigma$ -phase + Fe<sub>ss</sub> becomes continuous. In this case, the formation of TiFe and (Fe, Cr)<sub>2</sub>Ti reaction layers would prevent the Cr atoms from diffusing into brazed seam; thus, a large amount of Cr atoms segregated at the interface of brazed seam/316L, i.e., the interface of (Fe, Cr)<sub>2</sub>Ti layer/316L stainless steel, and the layer of  $\sigma$ -phase + Fe<sub>ss</sub> would become thicker during solidification.

**Fig. 15** Microstructure evolution: **a** sample assembly; **b** dissolution of base metals and atomic diffusion; **c** interfacial microstructure at elevated temperature; **d** terminal interfacial microstructure after solidification



## 4 Conclusions

TC4 titanium alloy was successfully brazed to 316L stainless steel with Ti-25Zr-50Cu amorphous filler metal. The effect of brazing time and temperature on the interfacial microstructure and mechanical properties of brazed joints was investigated and the main conclusions are drawn as follows.

- (1). The brazed seam consisted of three distinctive regions, and the typical interfacial microstructure of brazed joint was TC4 titanium substrate/Widmanstätten/ $\beta$ -Ti +  $\text{Ti}_2\text{Cu}/(\alpha\text{-Ti} + \lambda\text{-Cu}_2\text{TiZr}) + \text{Ti}_2\text{Cu}/\text{Ti-Fe-Cu}/\text{TiFe}/(\text{Fe}, \text{Cr})_2\text{Ti}/\sigma\text{-phase} + \text{Fe}_{\text{ss}}/316\text{L}$  stainless steel substrate.
- (2). Three thin reaction layers, i.e.,  $\text{TiFe}/(\text{Fe}, \text{Cr})_2\text{Ti}/\sigma\text{-phase} + \text{Fe}_{\text{ss}}$ , formed in the brazed joint close to 316L stainless steel substrate. These reaction phases were essentially brittle intermetallic compounds and determinative to the mechanical properties of joints. Increasing brazing time had no obvious effect on the morphology of these

reaction layers. And with the increase of brazing temperature, the total thickness of the layers increased and reached its maximum at 950 °C.

- (3). The shear strength of brazed joints first increased and then decreased with the increase of brazing time, whereas increasing brazing temperature could gradually improve shear strength of joints. The optimized brazing time was 10 min at brazing temperature of 930–950 °C. The maximum shear strength 65 MPa was obtained at 950 °C/10 min.
- (4). During shear test, the cracks initiated at the interface of Ti-Cu-Fe phase/TiFe phase, and propagated along the interface of brazed seam/316L ( $\text{TiFe}/(\text{Fe}, \text{Cr})_2\text{Ti}/\sigma\text{-phase} + \text{Fe}_{\text{ss}}$ ) with the secondary cracks spreading throughout the entire joints. The brittle fracture dominated the failure of joints with the presentation of a large amount of cleavage facets on the fracture surfaces. In addition, the mixed fracture modes of intergranular and transgranular existed on the fracture surfaces.

**Acknowledgements** The authors appreciate Professor Jian Cao at Harbin Institute of Technology in using a vacuum furnace. This work was technically supported by the Collaborative Innovation Center of Major Machine Manufacturing in Liaoning.

**Funding information** This work was financially supported by the National Key Research and Development Program of China (Program No. 2016YFB0701401) and the National Natural Science Foundation of China (Nos. 51674060 and 51605075).

**Publisher's note** Springer Nature remains neutral with regard to jurisdictional claims in published maps and institutional affiliations.

## References

- Wang SQ, Li WY, Zhou Y, Li X, Chen DL (2016) Tensile and fatigue behavior of electron beam welded dissimilar joints of Ti-6Al-4V and IMI834 titanium alloys. *Mat Sci Eng A* 649:146–152
- Zhou Y, Wen SF, Song B, Zhou X, Teng Q, Wei QS, Shi YS (2016) A novel titanium alloy manufactured by selective laser melting: microstructure, high temperature oxidation resistance. *Mater Des* 89:1199–1204
- Dong HG, Yu LZ, Deng DW, Zhou WL, Dong C (2015) Effect of post-weld heat treatment on properties of friction welded joint between TC4 titanium alloy and 40Cr steel rods. *J Mater Sci Technol* 31:962–968
- Dey HC, Ashfaq M, Bhaduri AK, Rao KP (2009) Joining of titanium to 304L stainless steel by friction welding. *J Mater Process Tech* 209:5862–5870
- Li P, Li JL, Salman M, Liang L, Xiong JT, Zhang FS (2014) Effect of friction time on mechanical and metallurgical properties of continuous drive friction welded Ti6Al4V/SUS321 joints. *Mater Des* 56:649–656
- Lee MK, Lee JG, Choi YH, Kim DW, Rhee CK, Lee YB, Hong SJ (2010) Interlayer engineering for dissimilar bonding of titanium to stainless steel. *Mater Lett* 64:1105–1108
- Kundu S, Anand G, Chatterjee S (2012) Diffusion bonding of 17-4 precipitation hardening stainless steel to Ti alloy with and without Ni alloy interlayer: interface microstructure and mechanical properties. *Metall Mater Trans A* 44:2196–2211
- Balasubramanian M (2015) Application of Box-Behnken design for fabrication of titanium alloy and 304 stainless steel joints with silver interlayer by diffusion bonding. *Mater Des* 77:161–169
- Elrefaey A, Tillmann W (2009) Solid state diffusion bonding of titanium to steel using a copper base alloy as interlayer. *J Mater Process Tech* 209:2746–2752
- Akbari Mousavi SAA, Farhadi Sartangi P (2009) Experimental investigation of explosive welding of cp-titanium/AISI 304 stainless steel. *Mater Des* 30:459–468
- Song J, Kostka A, Veehmayer M, Raabe D (2011) Hierarchical microstructure of explosive joints: example of titanium to steel cladding. *Mat Sci Eng A* 528:2641–2647
- Yadegari M, Ebrahimi AR, Karami A (2013) Effect of heat treatment on interface microstructure and bond strength in explosively welded Ti/304L stainless steel clad. *Mater Sci Tech-Lond* 29:69–75
- Tomashchuk I, Grevedy D, Sallamand P (2015) Dissimilar laser welding of AISI 316L stainless steel to Ti6-Al4-6V alloy via pure vanadium interlayer. *Mat Sci Eng A* 622:37–45
- Zhang Y, Sun DQ, Gu XY, Li HM (2016) A hybrid joint based on two kinds of bonding mechanisms for titanium alloy and stainless steel by pulsed laser welding. *Mater Lett* 185:152–155
- Tomashchuk I, Sallamand P, Belyavina N, Pilloz M (2013) Evolution of microstructures and mechanical properties during dissimilar electron beam welding of titanium alloy to stainless steel via copper interlayer. *Mat Sci Eng A* 585:114–122
- Wang T, Zhang BG, Wang HQ, Feng JC (2014) Microstructures and mechanical properties of electron beam-welded titanium-steel joints with vanadium, nickel, copper and silver filler metals. *J Mater Eng Perform* 23:1498–1504
- Jing Y, Yue X, Gao X, Su D, Hou J (2016) The influence of Zr content on the performance of TiZrCuNi brazing filler. *Mater Sci Eng A* 678:190–196
- Lee JG, Lee JK, Hong SM, Lee MK, Rhee CK (2010) Microstructure and bonding strength of titanium-to-stainless steel joints brazed using a Zr-Ti-Ni-Cu-Be amorphous filler alloy. *J Mater Sci* 45:6837–6840
- Cui J, Zhai QY, Xu JF, Wang YH, Ye JL (2014) Zr-Ti-Ni-Cu amorphous brazing fillers applied to brazing titanium TA2 and Q235 steel. *Mater Sci Appl* 05:823–829
- Dong HG, Yang ZL, Yang GS, Dong C (2013) Vacuum brazing of TiAl alloy to 40Cr steel with Ti60Ni22Cu10Zr8 alloy foil as filler metal. *Mat Sci Eng A* 561:252–258
- Dong HG, Yang ZL, Wang ZR, Deng DW, Dong C (2014) Vacuum brazing TC4 titanium alloy to 304 stainless steel with Cu-Ti-Ni-Zr-V amorphous alloy foil. *J Mater Eng Perform* 23:3770–3777
- Murray JL (1983) The Cu-Ti (copper-titanium) system. *Bull Alloy Phase Diagr* 4:81–95
- Bo H, Duarte LI, Zhu WJ, Liu LB, Liu HS, Jin ZP, Leinenbach C (2013) Experimental study and thermodynamic assessment of the Cu-Fe-Ti system. *Calphad* 40:24–33
- Botstein O, Rabinkin A (1994) Brazing of titanium-based alloys with amorphous 25wt.%Ti-25wt.%Zr-50wt.%Cu filler metal. *Mat Sci Eng A* 188:305–315
- Lee D-G, Lee S, Lee Y (2008) Effect of precipitates on damping capacity and mechanical properties of Ti-6Al-4V alloy. *Mat Sci Eng A* 486:19–26
- Xia YQ, Li P, Hao XH, Dong HG (2018) Interfacial microstructure and mechanical property of TC4 titanium alloy/316L stainless steel joint brazed with Ti-Zr-Cu-Ni-V amorphous filler metal. *J Manuf Process* 35:382–395
- Chiang W-R, Hsieh KC, Chang YA, Fan GJ, Qiao D, Qiao D, Jiang F, Liaw PK (2007) Phase equilibrium in the Cu-Ti-Zr system at 800°C. *Mater Trans* 48:1631–1634
- Liu CC, Ou CL, Shiue RK (2002) The microstructural observation and wettability study of brazing Ti-6Al-4V and 304 stainless steel using three braze alloys. *J Mater Sci* 37:2225–2235
- Sahlaoui H, Sidhom H (2013) Experimental investigation and analytical prediction of  $\sigma$ -phase precipitation in AISI 316L austenitic stainless steel. *Metall Mater Trans A* 44:3077–3083
- Lee TH, Oh CS, Lee CG, Kim SJ, Takaki S (2004) Precipitation of  $\sigma$ -phase in high-nitrogen austenitic 18Cr-18Mn-2Mo-0.9N stainless steel during isothermal aging. *Scripta Mater* 50:1325–1328
- Ghosh M, Bhanumurthy K, Kale GB, Krishnan J, Chatterjee S (2003) Diffusion bonding of titanium to 304 stainless steel. *J Nucl Mater* 322:235–241
- Shimada M, Kokawa H, Wang ZJ, Sato YS, Karibe I (2002) Optimization of grain boundary character distribution for intergranular corrosion resistant 304 stainless steel by twin-induced grain boundary engineering. *Acta Mater* 50:2331–2341
- Wang SS, Wang K, Chen GY, Li Z, Qin ZW, Lu XG, Li CH (2017) Thermodynamic modeling of Ti-Fe-Cr ternary system. *Calphad* 56:160–168
- Zhang HW, Cui W, He JS, Yan JC, Yang SQ (2015) Formation and evolution of intermetallic compounds at interfaces of Cu/Al joints by ultrasonic-assisted soldering. *J Mater Process Tech* 223:1–7
- Meshram SD, Mohandas T, Reddy G (2007) Friction welding of dissimilar pure metals. *J Mater Process Tech* 184:330–337